ACS OMEGA

Open Access

http://pubs.acs.org/journal/acsodf

Article

Nanocellulose/Fe_3O_4/Ag Nanozyme with Robust Peroxidase Activity for Enhanced Antibacterial and Wound Healing Applications

Seada Abdo Geleto, Abera Merga Ariti, Beamlak Teshome Gutema, Ebrahim M. Abda, Alfoalem Araba Abiye, Solomon M. Abay, Menbere Leul Mekonnen,* and Yitayal Admassu Workie*

Cite This: *ACS Omega* 2023, 8, 48764–48774

Read Online

ACCESS | Metrics & More | Article Recommendations | Supporting Information

ABSTRACT: Peroxidase memetic nanozymes with their free radical-mediated catalytic actions proved as efficacious antibacterial agents for combating bacterial resistance. Herein, nanocellulose (NC) extracted from *Eragrostis teff* straw was used to prepare NC/Fe_3O_4/Ag peroxidase nanozyme as an antibacterial and wound healing agent. Characterization of the nanozyme with XRD, FTIR, SEM-EDX, and XPS confirmed the presence of silver NPs and the magnetite phase of iron oxide dispersed on nanocellulose. The peroxidase activity of the prepared nanozyme was examined using TMB and H_2O_2 as substrates which turned blue in acidic pH (λ_{max} = 652 nm). With a lower K_m (0.387 mM), the nanozyme showed a comparable affinity for TMB with that reported for the HRP enzyme. Furthermore, the nanozyme remained efficient over a broader temperature range while maintaining 61.53% of its activity after the fourth cycle. In vitro, antibacterial tests against *Escherichia coli* (Gram-negative) and *Staphylococcus aureus* (Gram-positive) bacterial strains showed that NC/Fe_3O_4/Ag exhibits concentration-dependent and enhanced antibacterial effect for *Escherichia coli* compared to NC and NC-Fe_3O_4 and negative control. Furthermore, the wound-healing performance of the NC-Fe_3O_4−Ag nanozyme was investigated in vivo using an animal model (mice). The nanozyme showed 30% higher wound healing performance compared to the control base ointment and is comparable with the commercial nitrofurazone ointment. The results show the potential of the prepared nanozyme for wound-healing purposes.

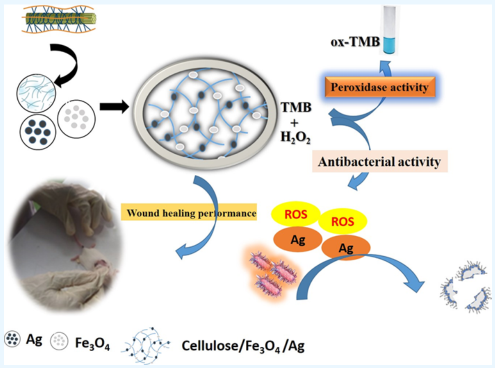

1. INTRODUCTION

Nanozymes are functional nanomaterials with enzyme-like activity. The inherent drawbacks of natural enzymes like poor stability, sensitivity to environmental conditions, and high cost of production limit their application.[1] To overcome this, artificial enzymes have been developed as stable, low-cost alternatives to natural enzymes called nanozymes.[2] Following the first report of Fe_3O_4 nanoparticles with peroxidase-like activity by Gao et al.,[3,4] in 2007, various nanozymes with unique enzyme-mimicking catalytic activities such as metal nanoparticles, metal oxide nanoparticles, and carbon-based nanomaterials (including carbon dots, graphite, graphene, and graphene oxide) have been reported as catalase,[5] peroxidase,[6] and oxidase,[7] mimicked activity.[8] Nanozymes are widely used in various applications such as imaging,[9] cancer diagnosis,[10] sensing,[11,12] and antibacterial wound healing activity.[13]

Globally, untreatable bacterial infections are on the rise due to the emergence of pathogens with multidrug resistance and the dearth of new antibiotic discoveries since 1980, prompting alternative therapies, such as bacteriophage therapy and antimicrobial enzymes.[14,15] Nanozymes, in particular, have great potential in combating antibacterial resistance due to their broad-spectrum antimicrobial properties.[16] Owing to their antibacterial mechanisms and physicochemical properties, nanozymes have great potential in combating antibacterial resistance.[16] Peroxidase mimetic nanozymes catalyze the conversion of hydrogen peroxide (H_2O_2) into highly toxic reactive oxygen species (ROS), such as hydroxyl radicals (·OH). The generated ROS attack the bacterial membranes of weakly acidic infection sites and kill them by destroying their cell membranes combating bacterial infections in wounds.[17,18] Although Fe_3O_4 NPs are commonly reported as peroxidase mimics,[19,20] their poor antibacterial activity limits their application for the treatment of infected wounds.[21] Therefore, metal nanoparticles such as silver can be coupled with Fe_3O_4 to enhance its antibacterial activity and wound-healing performance. Silver nanoparticles (Ag NPs) are known for their antibacterial effect and are used for bacterial infection and wound treatment.[22,23] Furthermore, the silver nanoparticle is reported to have a peroxidase-like activity which could enhance the antibacterial activity of magnetite NPs.[11,24] Despite their

Received: August 5, 2023
Revised: November 17, 2023
Accepted: November 30, 2023
Published: December 14, 2023

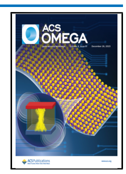

activity, Fe_3O_4 and Ag NPs are susceptible to aggregation, and this decreases their catalytic activity. To address this aggregation effect and sustain their activity, biopolymers such as cellulose, chitosan, chitin, etc., could be used as effective scaffolds to disperse the NPs. In addition, the hydroxyl and amino groups in these biopolymers could enhance the electron transfer similar to the amino acid microenvironments in natural enzymes.[25,26] Furthermore, nanocellulose has a unique morphology, high surface area and aspect ratio, quantum size effects, and other nanoscale properties that advance its biomedical applications.[27]

Yu et al.[28] synthesized a novel antibacterial agent based on Ag NPs and Fe_3O_4 loaded on chitin microspheres with peroxidase-like activity for synergistic antibacterial activity and wound healing. However, chitin in this work lacks hydrophilicity, which makes it difficult to maintain moisture and hence reduces its adhesiveness, which in turn makes the dressing less efficacious. Such problems could, however, be improved by using more hydrophilic scaffolds such as cellulose. Cellulose with its structural role, biocompatibility, and ability to absorb moisture could serve as an effective scaffold for wound healing.[22,29] In addition, the extended hydroxyl functional groups in the cellulose structure could enhance the electron transfer during the catalytic reaction rendering an amino acid microenvironment similar to the HRP enzyme.[30]

Hence, in this work, a nanocellulose/iron oxide/silver (NC-Fe_3O_4−Ag) nanocomposite was synthesized as a peroxidase mimetic nanozyme via the in situ redox reduction method. The synthesized nanocomposite was characterized using different state-of-the-art analytical techniques such as XRD, SEM-EDX, FTIR, and XPS which confirmed that magnetite and silver are attached to nanocellulose. The peroxidase activity of the nanozyme and the effects of various operational parameters were studied using 3,3′,5,5′-tetramethylbenzidine (TMB)/hydrogen peroxide (H_2O_2) substrates. The peroxidase activity test for the nanozyme indicated robust peroxidase activity with stronger substrate affinity. Furthermore, the antibacterial activity of the nanocellulose/iron oxide/silver (NC-Fe_3O_4−Ag) nanocomposite was studied in vitro against Gram-positive (*S. aureus*) and Gram-negative (*E. coli*) bacteria, and the wound healing performance was tested in vivo using an animal model (mice) yielding higher performance than a commercial antibacterial used as a control. The enhanced peroxidase activity and the consequent improved antibacterial effect are achieved due to the presence of cellulose, which serves as both a structural and functional scaffold.

2. EXPERIMENTAL SECTION

2.1. Materials. Glacial acetic acid (99.5%) and acetone (99%) were purchased from Sisco Research Laboratories, India. Sodium hydroxide (99.8%) was obtained from Central Drug House India. Sulfuric acid (98%), ammonium hydroxide (30%), ferric chloride (98%), and ferrous sulfate were obtained from Loba Chemie, India. Silver nitrate (99.9%) was purchased from Alpha Chemika, India. Hydrogen peroxide (30%), dimethyl sulfoxide (99.9%), sodium hypochlorite (5%), and ethanol (99.8%) were obtained from Research-LAB Fine Chem Industries India. Wool fat, hard paraffin, peptone, and sodium acetate were obtained from Sisco Research Laboratories, India. Sodium chloride was obtained from Rankem Chemical Industry, Delhi, India. Cetylstearyl alcohol, white soft paraffin, yeast, and agar media were purchased from Uni Chem Laboratories, Mumbai, India. The teff straw (*Eragrostesis teff*) was collected from Akaki Kality subcity, Addis Ababa, Ethiopia. All chemicals and reagents used for this experimental work were of analytical grade and were used without further purification.

2.2. Extraction of Nanocellulose. Cellulose was extracted from the teff straw (*Eragrostesis teff*) according to the previously reported method by Abdul Rahman et al.,[31,32] with slight modification. Briefly, the teff straw was collected and washed with distilled water. Then, it was air-dried for 10 days, followed by oven drying for 10 h at 50 °C. The teff straw was ground and sieved with a microsized sieve. Then, the teff straw powder (TSP) was treated with hot distilled water at 75 °C for 1 h with a fiber to water ratio of 1:20 (g: mL). The fiber was filtered with filter paper (Whatman filter paper No.1) and further treated with 4%w/v NaOH solution at 80 °C for 3 h under continuous stirring with the fiber to NaOH ratio of 1:20 (g: mL). The residue was vacuum-filtered and washed several times until the pH became neutral. Following, the fiber was subjected to a bleaching process by using acidified sodium hypochlorite solution (4% v/v) at 80 °C for 2 h under continuous stirring with a 1:20 (g: mL) ratio of fiber to acidified sodium chlorite solution. The pH of sodium hypochlorite was adjusted to 4 by glacial acetic acid. The process was repeated four times until the fiber turned white. Then, the residue was vacuum-filtered and washed several times with distilled water until the pH of the filtrate became neutral (pH 7). The final residue was oven-dried overnight at 50 °C and was kept for further experiment. Finally, nanocellulose (NC) was extracted according to the previously reported method[33] by hydrolyzing cellulose with sulfuric acid (48% v/v) solution under continuous stirring at 35 °C for 40 min with 1:25 (g: mL) ratio of fiber to the sulfuric acid solution. Then, 10-fold distilled water was added to the mixture to stop the hydrolysis process. The suspension was centrifuged at 3000 rpm for 5 min, washed three times with distilled water, freeze-dried for 24 h, and kept for further experiment.

2.3. Synthesis of the NC-Fe_3O_4−Ag Nanocomposite. The nanocellulose-iron oxide-silver (NC-Fe_3O_4−Ag) based nanocomposite was synthesized according to Wang et al., by in situ redox reaction.[34] Briefly, 7.447 g of $FeSO_4 \cdot 7H_2O$ was dissolved in distilled water. Then, 4 g of NC was immersed in the resultant aqueous solution, and the suspension was stirred for 1 h at room temperature. Subsequently, the suspension was heated to 90 °C and 10 mL of 1 M NaOH aqueous solution was added. Then the mixture was stirred at 90 °C for 2 min after adding 0.7874 g of $AgNO_3$. Finally, the NC-Fe_3O_4−Ag nanocomposite was centrifuged at 3000 rpm for 5 min, washed with distilled water until the pH became neutral, and freeze-dried for 24 h. Optimization of the precursor mass ratio was done by varying the concentration of each precursor at a time. Similarly, The NC-Fe_3O_4 was synthesized according to the previously reported method[35] by the in situ coprecipitation method. Briefly, 4 g of NC was dispersed in distilled water with stirring for 30 min. Then 2.8752 g of $FeCl_3$ was added and stirred for 1 h. After that 2.4824 g of $FeSO_4 \cdot 7H_2O$ was added and stirred for another 1 h. Subsequently, 10 mL of 30% NH_4OH solution was added dropwise and stirred for an hour until the mixture's color turned black which indicated the formation of Fe_3O_4 NPs particles, and oven-dried at 60 °C for 6 h. Different ratios of NC: Fe_3O_4 (for 1 g of NC, 0.25, 0.375, 0.5, and 0.625 g of Fe_3O_4) were optimized to select the best mass ratio of nanocomposite.

https://doi.org/10.1021/acsomega.3c05748
ACS Omega 2023, 8, 48764−48774

2.4. Characterization of the Nanozyme. Characterization of the nanozyme was performed using different state-of-the-art analytical techniques. The surface morphologies were investigated by a scanning electron microscope (SEM, FESEM, JSM-6500F JEOL), the crystallinity of the prepared nanomaterials was studied by X-ray diffraction (XRD-7000, DRAWELL), the elemental composition was studied using an X-ray photoelectron microscope (XPS, VG ESCA Scientific Theta Probe) with a monochromatic Al Kα X-ray source of 1486.6 eV), and the size of the prepared nanocomposite was studied by dynamic light scattering spectroscopy (DLS, Malvern). Fourier transform infrared spectroscopy (FT-IR, Nicolet Evolution-300) was used to confirm the functional groups, and UV−visible spectroscopy (UV−vis, JASCO 770) was used to study the optical properties of nanomaterials.

2.5. Peroxidase Mimetic Activity Test. The peroxidase-like activity of the synthesized nanomaterials was evaluated using 3,3′,5,5′- tetramethylbenzidine (TMB)/hydrogen peroxide (H_2O_2) substrates.[24] Briefly, 1.6 mg of nanozyme was dispersed in 3 mL of acetate buffer (pH 3.6), and 200 μL of TMB (6 mM) was added and incubated for 1 min. Then 200 μL of H_2O_2 (10 mM) was added and the reaction mixture was incubated for 2 min and the absorbance of the resulting blue-colored product from the oxidation of the chromogenic substrate was scanned from 200 to 800 nm. The effect of pH, temperature, the mass of nanozymes, time, and substrate concentration was optimized by varying each factor at a time. Furthermore, the steady-state kinetics of the prepared nanozymes was investigated by varying the concentration of TMB (0.25, 0.5, 0.75, 1, 1.25, 1.5, 1.75, and 2 mM) at a fixed concentration of H_2O_2 (10 mM) and varying the concentration of H_2O_2 (3, 4, 6, 8, 10, 12, and 14 mM) at a fixed concentration of TMB (3 mM). The resulting absorbance from the oxidation of TMB was measured at a fixed wavelength (652 nm) at a 5-s interval. The enzyme kinetic parameters were calculated from the Lineweaver−Burk plot (eq 1) which is the double-reciprocal plot derived from the Michaelis−Menten eq (eq 2).

$$\frac{1}{[v]} = \frac{k_m}{V_{max}}\frac{1}{[S]} + \frac{1}{V_{max}} \tag{1}$$

$$V = \frac{V_{max}[S]}{k_{m+[S]}} \tag{2}$$

where V is the initial velocity, V_{max} is the maximum velocity of the reaction, S is the initial concentration of the substrate, and K_m is the Michaelis constant which indicates the affinity of the enzyme to the substrate.

2.6. In Vitro Antibacterial Activity Test. The antibacterial activity of the prepared NC-Fe_3O_4−Ag nanocomposite was investigated using an LB agar media.[28,36] The selected bacterial strains (*E. coli* and *S. aureus*) were refreshed in Luria−Bertani (LB) medium (yeast extract, 5 g; tryptone, 10 g; NaCl, 5 g in 1 L of DI water, with the pH adjusted to 7.0 with NaOH) at 37 °C overnight. The bacterial suspension was diluted to 10^5 CFU/mL cells by using sterile phosphate-buffered saline (PBS, 0.01 mM, pH 7.4). Subsequently, NC, NC-Fe_3O_4 (nanocellulose−iron oxide), NC-Fe_3O_4−Ag, H_2O_2, NC-Fe_3O_4 + H_2O_2, NC-Fe_3O_4−Ag + H_2O_2 were placed into 2 mL bacterial suspensions and incubated at 37 °C for 2 h. Then 50 μL of the mixture was taken out and spread on a plate containing LB agar media and incubated at 37 °C for 24 h. As a positive control, chloramphenicol (30 μg) and as a negative control phosphate buffer (PB, 0.01 pH 6) were used. Then, different concentration of NC-Fe_3O_4−Ag nanocomposite (25, 50, 100, 150 μg/mL) was studied to test the effect of concentration on antibacterial activity. Finally, bacterial colonies on the culture plate were counted to test the percent survival of the two bacteria, *E. coli* and *S. aureus*.

2.7. In Vivo Evaluation of the Wound Healing Performance Test. Animals were obtained from the animal house of the School of Pharmacy, Addis Ababa University, Ethiopia. The wound healing performance test and dermal toxicity were performed by selecting 4−5 week healthy sex Swiss albino mice (25−35 g). They were housed in cages under standard conditions (22 ± 3 °C and 12 h light and dark cycles) and given a standard pellet diet and water. They were acclimatized to the laboratory conditions for a week before the experiment and they were handled according to the International Guidelines for the Use and Care of Laboratory Animals.[13,29]

2.8. Dermal Toxicity Test. Dermal toxicity was studied using five female mice according to the Organization for Economic-Co-operation and Development (OECD) Guideline.[37] Following acclimatization for 7 days, the mice were anesthetized with a ketamine (50 mg/kg) (intraperitoneal (I.P.)) injection and sedated with diazepam (1 mg/kg). A diameter of 2 cm of fur was shaved on the back of mice as indicated in the photograph in Figure S1.[17] The base ointment was prepared according to the British Pharmacopoeia (BP, 2018) using wool fat, hard paraffin, cetylstearyl alcohol, and white soft paraffin with a formula described in Table S1. Then 0.5 and 1% of NC-Fe_3O_4−Ag and NC-Fe_3O_4−Ag + H_2O_2 of the prepared base ointment were applied, and then animals were returned to individual cages. The skin irritation was visually inspected for 14 days with an interval of 24 h. The skin irritation was evaluated by calculating the primary irritation index (PII) as per eq 3. The degree of irritation of nanomaterials was categorized as negligibly irritant (PII of <0.5), mildly irritant (PII of 0.5−1.9), moderately irritant (PII of 2−5), and severely irritant (PII of >5).[17]

$$\text{PII} = \frac{\Sigma\ \text{Erythema and Edema grade at 1, 24, 48 and 72 h}}{\text{No. of test sites} \times 4\ \text{scoring intervals}} \tag{3}$$

2.9. Bacterial Infected Wound Healing Performance Test. In vivo, antibacterial and wound healing performance tests were performed using 5 weeks aged either sex *albino* mice.[28] Following the random division of mice into six groups (six mice in each group): group I is a nonmedicated (base) ointment and served as a negative control, the second group (group II) mouse received 0.2% (w/w) ointment of the standard drug (Nitrofurazone), as a positive control. Mouse in groups III, IV, V, and VI were treated with NC, H_2O_2, NC-Fe_3O_4−Ag, and NC-Fe_3O_4−Ag + H_2O_2 respectively. Negative control, positive control, NC, H_2O_2, NC-Fe_3O_4−Ag, and NC-Fe_3O_4−Ag + H_2O_2 treated mice were anesthetized and sedated with an intraperitoneal (ip) injection of ketamine (50 mg/kg) and diazepam (1 mg/kg) correspondingly. A wound with about 2 cm diameter was created by removing dorsal flank skin on the back of the mice and infected with *E. coli* (200 μ L, 1 × 10^5 CFU/ml) to build a wound infection model and H_2O_2, 0.5 and 1% of NC, NC-Fe_3O_4−Ag and NC-Fe_3O_4−Ag + H_2O_2

https://doi.org/10.1021/acsomega.3c05748
ACS Omega 2023, 8, 48764−48774

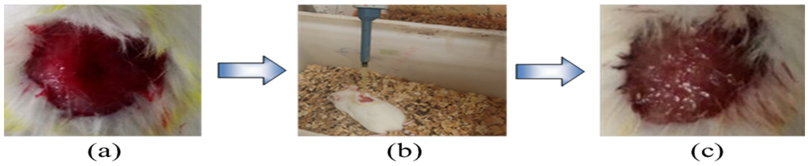

Figure 1. Photographic images of mice (a) wound created; (b) applying bacteria on the created wound; (c) infected wound (photo taken by Seada Abdo Geleto Copyright 2023).

were applied in the first day considered as day 0 as shown in Figure 1. After 24 h, controls and nanozymes were applied, and then animals were returned to cages and provided with food and water. The wounds were photographed on days 1, 2, 4, 6, 8, and 14 wound areas were measured to calculate the wound contraction. Furthermore, the bacterial samples were taken from the wound area on day 3 and spread onto sterilized saline water. Then, the suspension was spread on LB agar and kept at 37 °C for 24 h to evaluate in vivo antibacterial activity.[20]

3. RESULTS AND DISCUSSION

3.1. Extraction of Nanocellulose. Cellulose was extracted and optimized from *Eragrostesis teff* straw using alkali treatment followed by hypochlorite bleaching as indicated in Figure S2. The volume of 1 M NaOH and reaction temperature were optimized yielding 33.6% of cellulose. Nanocellulose was then obtained by the acid hydrolysis of cellulose. The percentage yield obtained in this work is higher than previously reported work.[33]

3.2. Synthesis and Characterization of the NC-Fe_3O_4–Ag Nanocomposite. The surface morphology of nanocellulose and nanocomposite was characterized by SEM-EDX. As shown in Figure 2A(a), the flake structures of nanocellulose

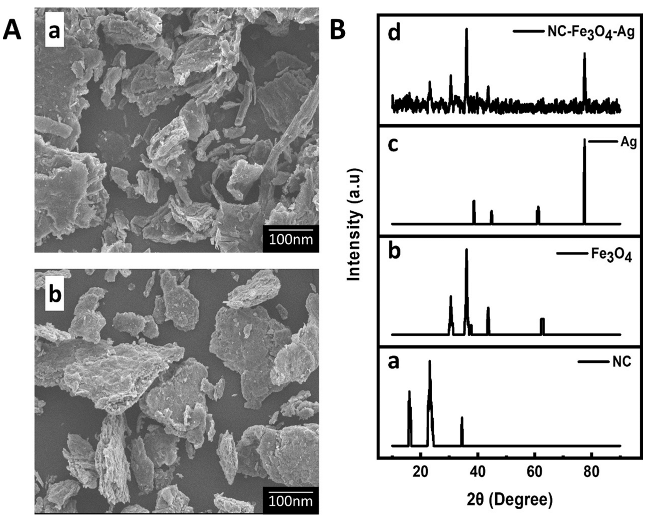

Figure 2. (A) SEM micrographs of (a) nanocellulose; (b) NC-Fe_3O_4–Ag nanocomposite; (B) XRD pattern of (a) nanocellulose; (b) Fe_3O_4 NPs; (c) Ag NPs; (d) NC-Fe_3O_4–Ag.

are observed, indicating the success of the extraction process. Further, as seen in the SEM micrograph of NC-Fe_3O_4–Ag (Figure 2A(b)), the nanoparticles are embedded on the surface of flake nanocellulose. The EDX spectrum and elemental mapping in Figure S3 show the presence of C, O, Ag, and Fe which are the expected elemental compositions of the prepared nanocomposite.

The crystallinity and phase composition of the prepared nanocomposite were checked by powered XRD. As illustrated in Figure 2B(a). the peaks at 2θ of 16, 22, and 34° represent diffractions from cellulose nanofiber (110), (200) and (040) planes, respectively.[38] As shown in (b), the diffractions peak at 2θ 30.2, 35.4, 43.2, and 57.2° and correspond to (220), (311), (400), and (511) planes of magnetite (Fe_3O_4) phase, respectively. The peaks are consistent with JCPDF No. 65–3107 and reveal the formation of a pure Fe_3O_4 phase. While the peaks at 2θ of 38.36 and 44.5° can be assigned to diffractions from (111) and (200) planes of crystalline cubic Ag NPs (JCPDS card no. 04–0783) (Figure 2B(c)). All these characteristic peaks appeared in the nanocomposites, as presented in Figure 2B(d). Furthermore, the crystallite size of NC, Fe_3O_4, and Ag was calculated from the XRD patterns using the Debye-Scherer equation and is found to be 16.94 17.45, and 18.08 nm, respectively.

Further, the chemical states and compositions of NC-Fe_3O_4–Ag were analyzed using XPS. The wide scan XPS spectrum (Figure 3A(a)) indicates the presence of Fe, Ag, O, and C which are consistent with the precursor's compositions. The high-resolution XPS spectrum of Fe 2p (Figure 3A(b)) indicates two peaks at BE 710.1 and 723.5 eV which represents Fe $2p_{3/2}$ and Fe $2p_{1/2}$ from Fe_3O_4. The narrow scan XPS spectrum (Figure 3A(c)) shows two peaks at BE 367 and 373 eV which are characteristics of Ag $3d_{5/2}$ and Ag $3d_{3/2}$ electrons. The results are consistent with the XRD data and confirm the presence of Fe_3O_4 and Ag NPs in the cellulose structure. The percentage of Fe and Ag calculated from the XPS data are 15.54 and 14.87% respectively. This result is also in line with the previously reported study.[39]

The functional groups present at different stages of synthesis were investigated by FTIR. As shown in Figure 3B(a,b), the broad peak at 3400 cm^{-1} corresponds to the OH stretching. The sharp peak at 1180 cm^{-1} represents the C–O–C stretching of the glyosidic bond in NC. While on the FTIR spectrum of the composite (Figure 3B(c,d)), a new weak peak appeared at 590 cm^{-1} that can be assigned to the stretching of Fe–O bonds, indicating the association of Fe in the NC structure. The wavenumbers and functional groups of the nanomaterials are listed in Table S2.

3.3. Peroxidase Memetic Activity of the Nanozyme. The preliminary peroxidase activity of nanocellulose (NC), nanocellulose-iron oxide (NC-Fe_3O_4), and nanocellulose-iron oxide- silver (NC-Fe_3O_4–Ag) nanocomposite was investigated using the chromogenic reaction of the H_2O_2-TMB system in an acetate buffer (pH 3.6). The absorbance of the resulting reaction product was then measured using a UV–visible spectrometer. As shown in Figure 4A(a), the addition of H_2O_2-TMB to the nanozyme resulted in a blue color with characteristics of absorption at 652 nm indicating the catalytic oxidation of the TMB. However, when TMB and H_2O_2 are allowed to react alone, the expected blue color was not observed confirming the role of the nanozyme in the catalytic

https://doi.org/10.1021/acsomega.3c05748
ACS Omega 2023, 8, 48764–48774

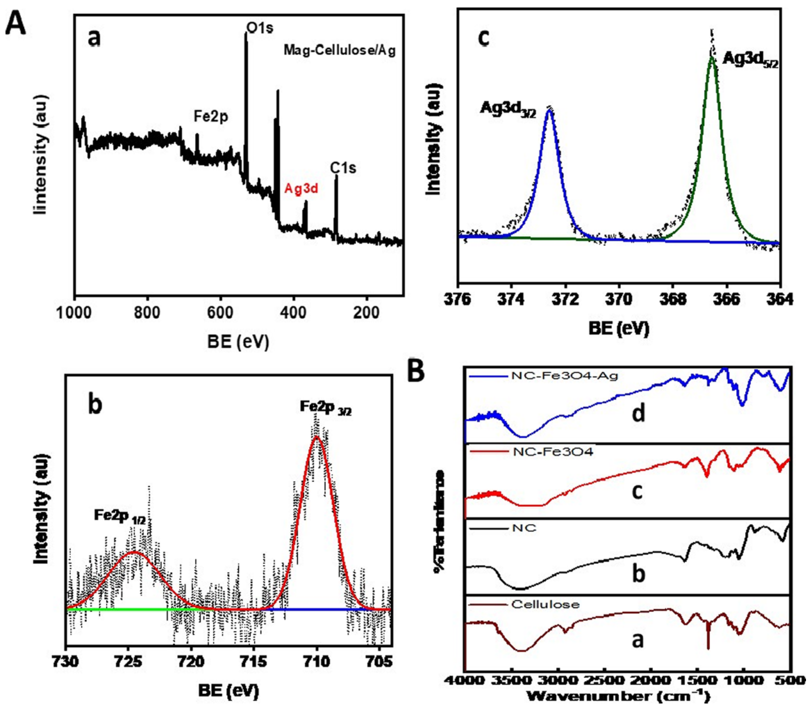

Figure 3. (A) (a) Wide scan XPS spectrum of NC-Fe_3O_4–Ag nanocomposite; high-resolution XPS spectrum for (b) Fe 2p; (c) Ag 3d. (B) FT-IR spectrum of (a) commercial cellulose; (b) NC; (c) NC-Fe_3O_4; and (d) NC-Fe_3O_4–Ag nanocomposite.

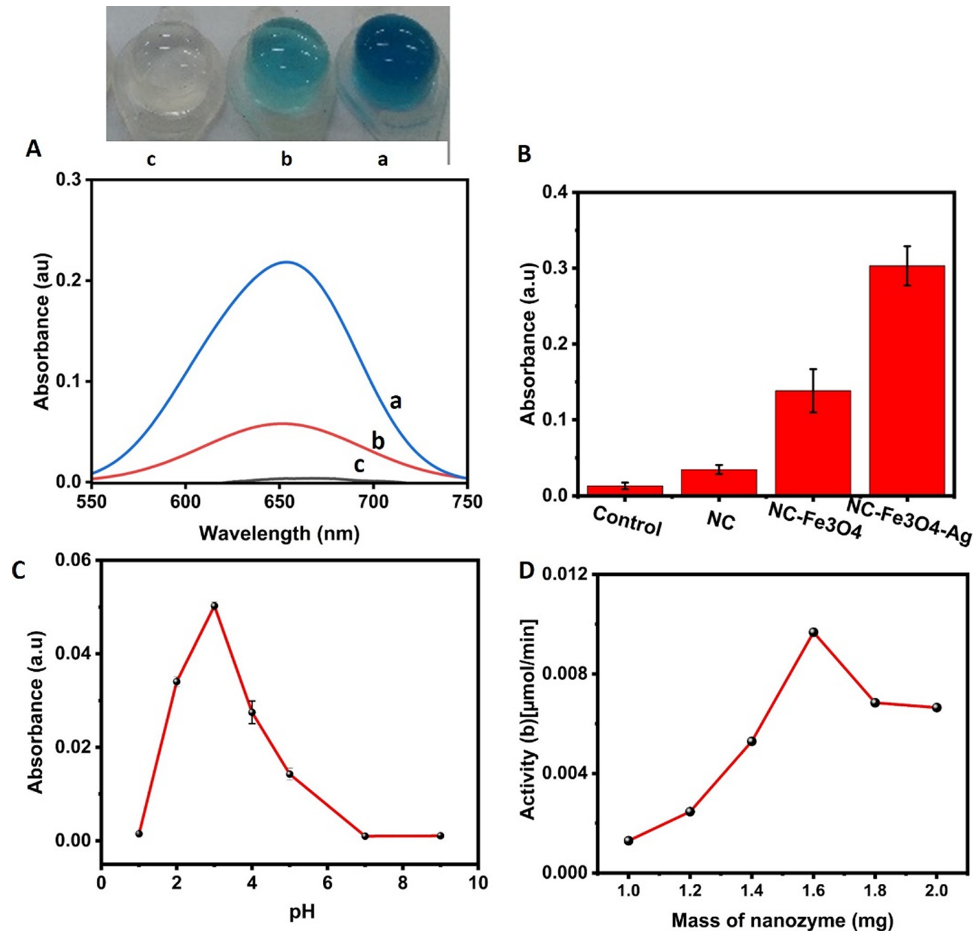

Figure 4. (A) Preliminary peroxidase activity tests for NC-Fe_3O_4–Ag nanocomposite; (a) TMB + H_2O_2+ nanozyme; (b) buffer + TMB + H_2O_2; (c) TMB + H_2O_2; (B) comparison of peroxidase activity of nanozymes; (C) effect of pH; (D) effect of nanozyme mass on the peroxidase activity.

https://doi.org/10.1021/acsomega.3c05748
ACS Omega 2023, 8, 48764−48774

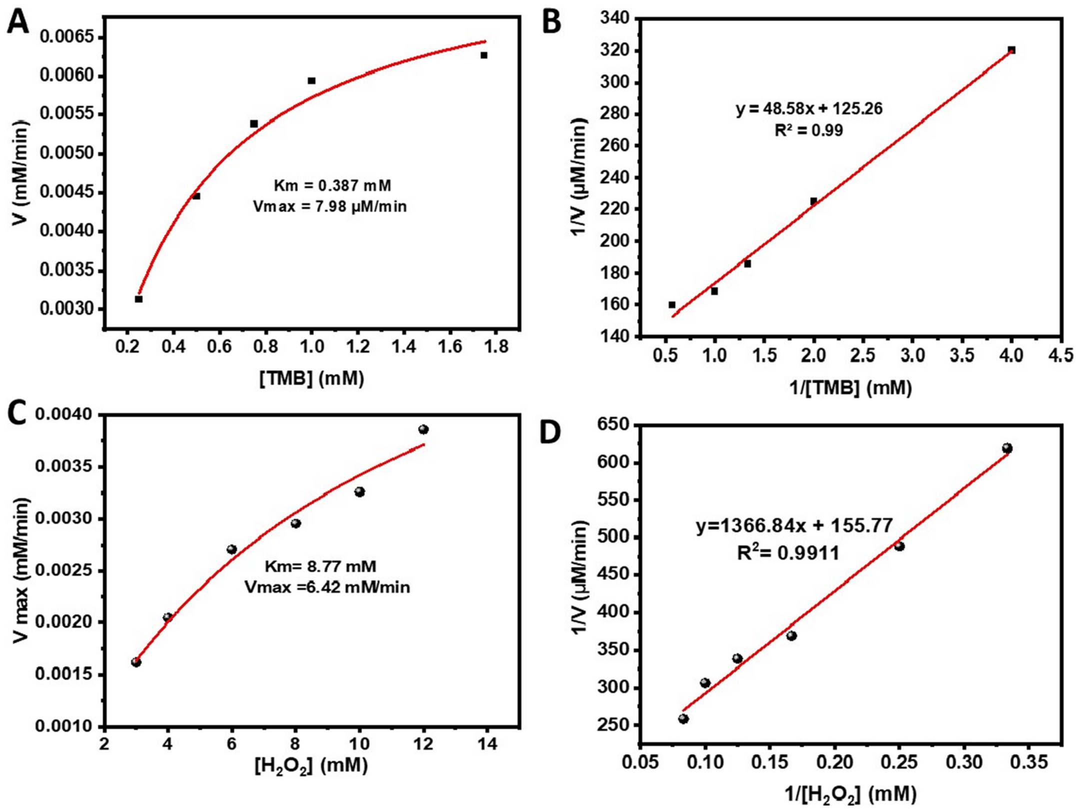

Figure 5. Michaelis−Menten curve: (A) TMB; (C) H_2O_2. Lineweaver−Burk plot: (B) TMB; (D) H_2O_2.

reactions (Figure 4A(c)). The buffer, however, induces slight oxidation of TMB which could be due to protonation of the TMB (Figure 4A(b)). The value of this buffer effect was subtracted in the subsequent assay. The effect of the precursor mass ratio was optimized as shown in Figure S4.

Furthermore, as seen in Figure 4B, nanocellulose alone did not show significant peroxidase activity while the addition of Ag NPs resulted in 47.8% higher activity than NC-Fe_3O_4 which could be attributed to the synergetic effect of the two nanoparticles. The pH of the medium is an important factor for the enzymatic activity. Hence, the peroxidase mimicking activity of the developed nanozyme was studied at different pH. As illustrated in Figure 4C, the synthesized nanozyme effectively functions in acidic pH, reaching its optimum at pH 3.6. This highest activity of the nanocomposite in acidic conditions could be due to the protonation of surfaces which enhances the oxidation of TMB. However, as the pH gets lower, the color of the solution turns yellowish indicating the complete oxidation of TMB into its diamine cation.[2]

As shown in Figure 4D, 1.6 mg of the nanozyme resulted in the highest activity, which was used for the next experiments. The specific activity was then calculated from the slope of the plot of *unit activity (b) vs mass of nanozyme* The unit activity was calculated using eq 4 from the initial rate measurement. Accordingly, the specific activity was calculated to be 0.01398 U/mg where $U = \mu$mol/min mg (Figure S5).

$$b_{\text{nanozyme}} = \frac{V}{\varepsilon l} \times \frac{\Delta A}{\Delta t} \tag{4}$$

where b is unit activity of the nanozymes [μmol/minL], V is volume (μL), ε is the absorptivity coefficient (12,800 M^{-1} cm^{-1}), and l is thepath length (1 cm) for initial rates of the reaction. The effect of H_2O_2 concentration was also investigated by varying its concentration at a fixed nanozyme mass and TMB Concentration. As seen in Figure S6, the peroxidase activity increase with concentration of H_2O_2 up to 10 mM stayed constant after that. Hence this concentration was chosen for the rest of the experiments.

3.4. Steady-State Kinetics Study. Furthermore, the steady-state kinetics were studied by varying the concentration of each substrate at a time at a fixed dose of the nanozyme. As seen in Figure 5A,C the catalytic reactions obey the typical Michaelis−Menten model. The kinetic parameters such as K_m and V_{max} were then calculated from the Lineweaver−Burk plots (Figure 5B,D). Accordingly, the K_m and V_{max} were found to be 0.387 and 7.98 μM/min for TMB and 8.77 and 6.42 μM/min for H_2O_2 respectively showing strong substrate affinity. Further, as seen in Table S3, the prepared nanozyme has a lower binding affinity for TMB than the natural HRP enzyme reported before. Furthermore, the bimetallic nanozyme showed higher catalytic turnover than the monometallic one, which could be due to the synergetic catalytic effect (Table 1 and Figure S7).

3.5. Stability and Recyclability of the Nanozyme. The thermal stability of the nanozyme was examined by conducting the peroxidase memetic assay at different temperatures (25, 35, 50, 65, 80, and 90 °C) in a water bath system. As shown in

Table 1. Kinetic Parameters of the Prepared Nanozymes

naozyme	substrate	K_m (mM)	V_{max} (μM/min)	K_{cat} (min^{-1})
NC-Fe_3O_4	TMB	5.14	2.72	0.6
	H_2O_2	1.8	4.7	1.1
NC-Fe_3O_4−Ag	TMB	0.387	7.98	1.8
	H_2O_2	8.77	6.42	1.4

https://doi.org/10.1021/acsomega.3c05748
ACS Omega 2023, 8, 48764−48774

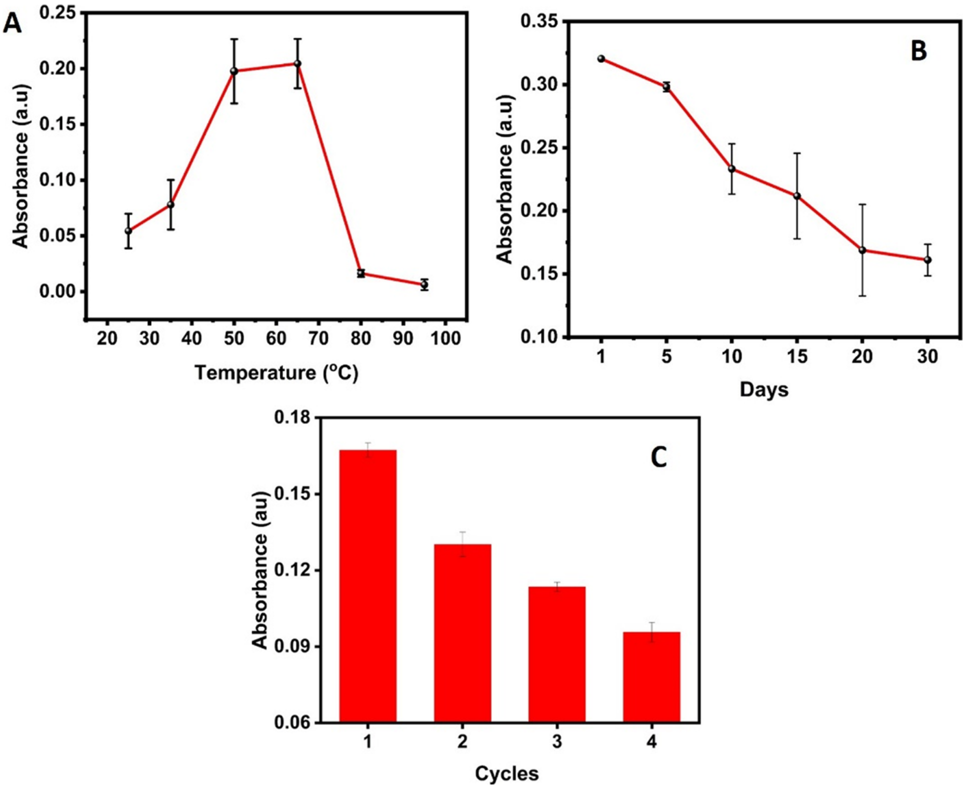

Figure 6. (A) Thermal stability; (B) temporal stability; (C) recyclability of the nanozyme.

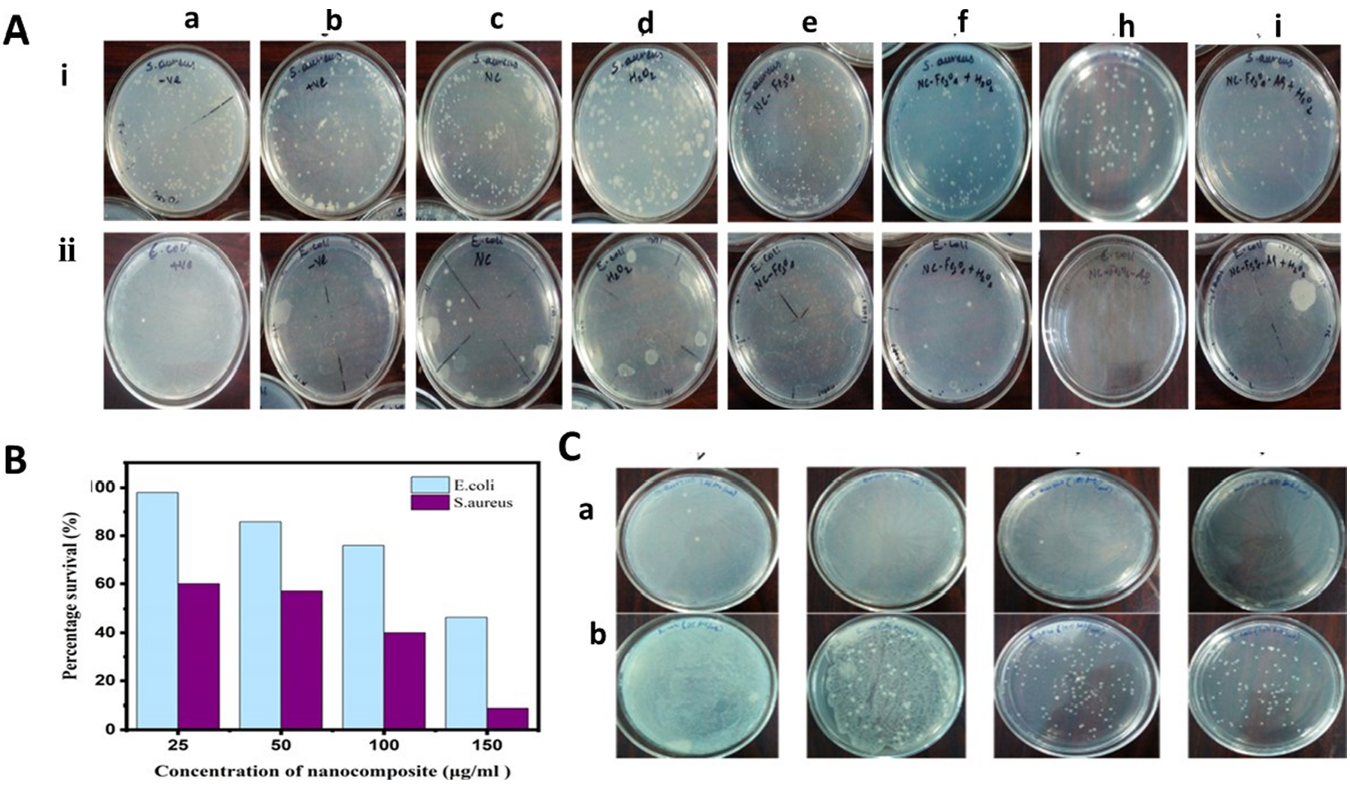

Figure 7. (A) In vitro antibacterial activity; (B) percentage survival; (C) effect of concentration on antibacterial activity of the nanozyme (photo taken by Seada Abdo Gelet Copyright 2023).

Figure 6A, the peroxidase memetic activity increases until the temperature reaches 65 °C and declines afterward retaining 50% of its room temperature activity at 80 °C. In addition, the temporal stability of NC-Fe_3O_4–Ag nanozyme was also investigated for 30 days by keeping it at room temperature and dispersed in the buffer. As seen in Figure 6B, the

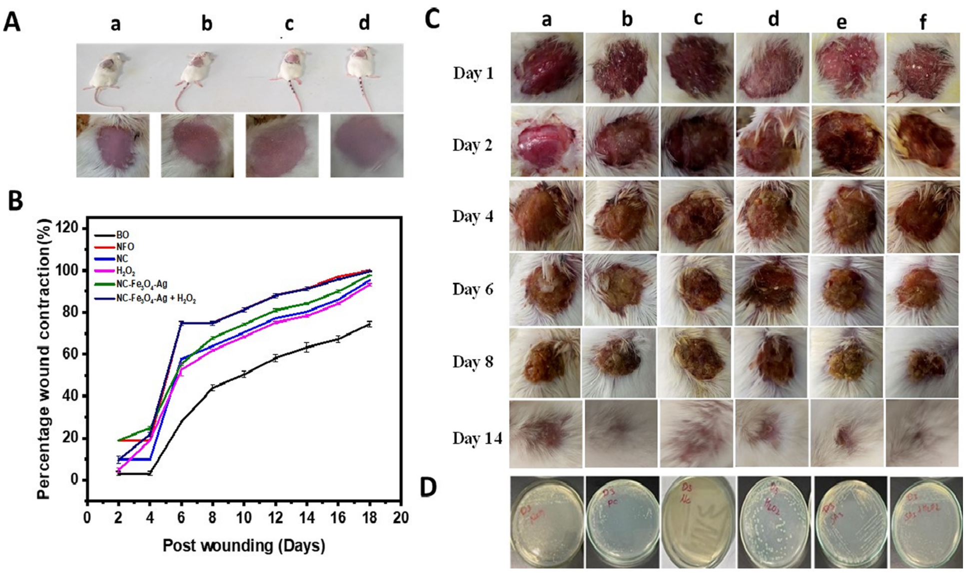

Figure 8. (A) Dermal toxicity effect; (B) percentage of wound contraction; (C) digital images of the wound healing process; (D) antibacterial test result from back culture (photo taken by Seada Abdo Geleto Copyright 2023).

nanozyme retains 32% of its original activity even after 30 days of storage. Both thermal and temporal stability test results signify a robust performance of the prepared nanozyme, which rivals the natural enzymes.

Recyclability is also another important factor required for the practical application of nanozymes. The peroxidase metic activity of the recovered NC-Fe_3O_4–Ag nanozyme was studied for four successive cycles. The recovered nanozyme was washed with distilled water before each cycle of the assay. As illustrated in Figure 6C, the nanozyme maintained its 61.53% peroxidase activity after the fourth cycle suggesting excellent performance.

3.6. Antibacterial Activity Test. The in vitro antibacterial activity of the prepared materials (NC, H_2O_2, NC-Fe_3O_4, NC-Fe_3O_4 + H_2O_2, NC-Fe_3O_4–Ag, NC-Fe_3O_4–Ag + H_2O_2) was examined against Gram-negative (*E. coli*) and Gram-positive (*S. aureus*) bacteria using LB agar media. As presented in Figure 7A(i,ii(a)), the negative control plate (phosphate bufer, pH 6), remained turbid and did not show any antibacterial activity. As presented in Figure 7A(i,ii(b)), the positive control Chloramphenicol showed better antibacterial effect against Gram-negative bacteria (*E. coli*). However, the bacterial colonies of *S. aureus* (Figure 7A(i)) and *E. coli* (Figure 7A(ii)) bacteria decreased and still remained turbid for the plates containing NC (Figure 7A(i,ii(c))), H_2O_2 (Figure 7A(i,ii-(i,ii(d))), NC-Fe_3O_4 (Figure 7A(i,ii(e))), and NC-Fe_3O_4 + H_2O_2 (Figure 7A(i,ii(f))). The prepared nanocomposite NC-Fe_3O_4–Ag (Figure 7A(i,ii(g))) displayed the highest antibacterial activity compared to other nanomaterials.

Correspondingly, the synergetic effect happens when H_2O_2 is added to NC-Fe_3O_4–Ag nanozyme and the plate becomes clear (Figure 7A(i,ii(h))). Thus, the nanozyme is more effective against *S. aureus* than against *E. coli*. The main reason for leading to the synergistic antibacterial activity of nanozyme when mixed with H_2O_2 is due to the presence of Ag NPs on nanozyme which can release Ag^+ that can interact with bacteria and exert its effect. The other reason is due to the ability of nanozyme (NC-Fe_3O_4–Ag) to effectively catalyze H_2O_2 to generate a hydroxyl radical, or ROS which can damage the cell membrane of bacteria. In addition, Ag NPs are well-known antibacterial agents and their presence enhances the peroxidase mimicking activity of the nanozyme as well as its effect against bacteria. Furthermore, the percentage survival of *S. aureus* and *E. coli* after the treatment with different concentrations (25 μg/mL, 50 μg/mL, 100 μg/mL, 150 μg/mL) of nanozyme (NC-Fe_3O_4–Ag) was examined as presented in Figure 7B. As seen in Figure 7C, the growth of both strains of bacteria was inhibited with an increase in the concentration of the nanozyme, and at 150 μg/mL, a very clear plate was observed for *E. coli* (Figure 7C(b)) than *S. aureus* (Figure 7C(a)).

3.7. In Vivo Wound Healing Performance Test. The dermal toxicity of the nanozyme was determined by the standard protocol on mice. As shown in Figure 8A, nanozyme (NC-Fe_3O_4–Ag) with and without H_2O_2 did not cause any irritation, inflammation, and edema irritation even with the maximum ointment dose (1%). The PII value was obtained to be <0.5 which indicates negligible irritation of nanozyme to mice skin. Therefore, this nanozyme is safe and biocompatible for the preparation of ointment-based wound dressing.

Following the dermal toxicity result, the wound healing ability of NC, H_2O_2, NC-Fe_3O_4–Ag, and NC-Fe_3O_4–Ag + H_2O_2 was examined *vivo* on animal models (mice). Initially, the wound was created, infected, and photographed, and its area was measured as presented in Figure 8C. Then, the infected mice were divided into six groups: (based ointment) (control group) (Figure 8C(a)), nitrofurazone (positive control) group (Figure 8C(b)), (NC) group (Figure 8C(c)), (H_2O_2) group (Figure 8C(d)), (NC-Fe_3O_4–Ag) group (Figure 8C(e)), and (NC-Fe_3O_4–Ag + H_2O_2) group (Figure 8C(f)). The wounds were photographed on the first, second, fourth, sixth, eighth, and 14th day. Accordingly, the size of the wound started to decrease on the second day for all treatment groups except the control group (base ointment). During the treatment period, the progress of healing of the infected wound was measured, and the percentage contraction is presented in Figure 8B. As illustrated in Figure 8B,C, on the eighth day of treatment, the control group (base ointment) shows about 40% wound contraction. Interestingly, the nanozyme group (NC-Fe_3O_4–Ag) showed 68% wound contraction (Figure 8C(e)) and the positive control (nitrofurazone) group showed

https://doi.org/10.1021/acsomega.3c05748
ACS Omega 2023, 8, 48764–48774

75% wound contraction healing performance (Figure 8C(b)) which indicates the effectiveness of the prepared nanozyme for the wound healing application. This could be ascribed to the moisture-absorbing ability of nanocellulose and the intrinsic antibacterial activity of Ag NPs which together enhance wound healing process.[28] The NC-Fe_3O_4−Ag + H_2O_2 group (Figure 8C(f)), shows about 76% wound contraction, which is higher than the positive control (nitrofurazone) group. This could be due to the presence of H_2O_2 which could induce ROS generation and hence promote peroxidase-based antibacterial action. Thus, the result (NC-Fe_3O_4−Ag + H_2O_2) group shows more than 30% wound contraction on day 8 compared to the control group (base ointment) group in which wound contraction is due to its natural wound healing process. Further, on the 14th day, the nanozyme causes complete healing similar to that of the nitrofurazone group. Therefore, the wound healing process significantly accelerates and reduces the healing time. Overall, the prepared nanozymes are effective for wound healing applications.

Furthermore, to verify the antibacterial activity of nanomaterials, the bacteria on the wound site was back cultured on the third day (Figure 8D). The bacteria remain on the base ointment (Figure 8D(a)), nanocellulose (Figure 8D(c)), and H_2O_2 group (Figure 8D(d)), whereas the NC-Fe_3O_4−Ag) (Figure 8D(e)) and (NC-Fe_3O_4−Ag + H_2O_2) (Figure 8D(f)) groups resulted in cleared plates comparable with the positive control group (Figure 8D(b)), indicating the synergistic antibacterial effect which resulted in efficient wound healing performance.

4. CONCLUSIONS

In summary, nanocellulose was extracted from *Eragrostis tef straw,* and a nanocellulose/iron oxide/silver (NC/Fe_3O_4/Ag) nanocomposite was successfully prepared by the in situ redox method and characterized by XPS, XRD, and SEM-EDX. Morphological and structural characterizations confirmed the formation of magnetite and silver nanoparticles on the surface of nanocellulose. The prepared nanozyme showed peroxidase memetic activity, and the antibacterial healing performance of the nanozyme was investigated. The nanozyme showed robust peroxidase memetic activity in acidic conditions at as high temperatures as 65 °C. The peroxidase memetic activity in catalyzing the chromogenic reactions between TMB and H_2O_2 followed a typical Michaelis−Menten model with a higher affinity for TMB than a previously reported natural HRP enzyme. Besides, the addition of silver showed a synergistic catalytic effect resulting in a 47.8% improved peroxidase activity on NC/Fe_3O_4. The antibacterial activity of NC/Fe_3O_4/Ag was examined in vitro using selected Gram-negative (*Escherichia coli*) and Gram-positive (*Staphylococcus aureus*) bacterial strains. The nanozyme showed high antibacterial activity toward both bacterial strains. Furthermore, the wound healing performance of the synthesized NC/Fe_3O_4/Ag ointment-based antibacterial wound healing was investigated in vivo using animal models (mice). Accordingly, the nanozyme showed 76% wound contraction, which is more than 30% higher than the negative control. Overall, the prepared nanozyme revealed promising peroxidase memetic activity and antibacterial performance.

■ ASSOCIATED CONTENT

Data Availability Statement

Data will be made available on request.

Supporting Information

The Supporting Information is available free of charge at https://pubs.acs.org/doi/10.1021/acsomega.3c05748.

> Photographic images of anesthetized, shaved, and nanocomposite-based ointment applied on mice; extraction of nanocellulose and the effect of volume and temperature on cellulose extraction; EDX and mapping spectrum of NC-Fe_3O_4−Ag; optimization of the precursor ratio of NC-Fe_3O_4 and NC-Fe_3O_4−Ag; unit activity of NC-Fe_3O_4−Ag; effect of H_2O_2 concentration; kinetic parameter comparison and Michaelis−Menten plot for monometallic nanozyme; preparation of the ointment according to British Pharmacopoeia; wavenumbers and functional groups in cellulose, NC, NC-Fe_3O_4, and NC-Fe_3O_4−Ag nanocomposite; and K_m and V_{max} values of NC-Fe_3O_4−Ag and recently reported peroxidase mimicking nanozymes (PDF)

■ AUTHOR INFORMATION

Corresponding Authors

Menbere Leul Mekonnen − *Industrial Chemistry Department, Addis Ababa Science and Technology University, Addis Ababa 1647, Ethiopia; Nanotechnology Center of Excellence, Addis Ababa Science and Technology University, Addis Ababa 1647, Ethiopia;* orcid.org/0000-0001-9617-853X; Email: menbere.leul@aastu.edu.et

Yitayal Admassu Workie − *Industrial Chemistry Department, Addis Ababa Science and Technology University, Addis Ababa 1647, Ethiopia; Nanotechnology Center of Excellence, Addis Ababa Science and Technology University, Addis Ababa 1647, Ethiopia*; Email: yitayal.admasu@aastu.edu.et

Authors

Seada Abdo Geleto − *Industrial Chemistry Department, Addis Ababa Science and Technology University, Addis Ababa 1647, Ethiopia*

Abera Merga Ariti − *Industrial Chemistry Department, Addis Ababa Science and Technology University, Addis Ababa 1647, Ethiopia*

Beamlak Teshome Gutema − *Biotechnology Department, Addis Ababa Science and Technology University, Addis Ababa 1647, Ethiopia*

Ebrahim M. Abda − *Biotechnology Department and Bioprocess and Biotechnology Center of Excellence, Addis Ababa Science and Technology University, Addis Ababa 1647, Ethiopia*

Alfoalem Araba Abiye − *Department of Pharmacology and Clinical Pharmacy, School of Pharmacy, College of Health Sciences, Addis Ababa University, Addis Ababa 1647, Ethiopia*

Solomon M. Abay − *Department of Pharmacology and Clinical Pharmacy, School of Pharmacy, College of Health Sciences, Addis Ababa University, Addis Ababa 1647, Ethiopia*

Complete contact information is available at: https://pubs.acs.org/10.1021/acsomega.3c05748

Author Contributions

S.A.G.: investigation, material preparation, writing—original draft, software. A.M.A.: investigation, material characterization. B.T.G.: investigation, material characterization. E.M.A.: conceptualization, supervision. M.L.M.: conceptualization, funding acquisition, resources, methodology, writing—review and editing. Y.A.W.: conceptualization, supervision, methodology, writing—review and editing.

Notes

The authors declare no competing financial interest.
All animal experimental procedures were conducted according to the ethical regulations of the Department of Pharmacology and Clinical Pharmacy, Addis Ababa University, Ethiopia.

■ ACKNOWLEDGMENTS

The authors are grateful to Addis Ababa Science and Technology University for the financial and facility support through its internal interdisciplinary research grant (IG07/22).

■ REFERENCES

(1) Huang, Y.; Ren, J.; Qu, X. Nanozymes: Classification, Catalytic Mechanisms, Activity Regulation, and Applications. *Chem. Rev.* **2019**, *119* (6), 4357−4412.
(2) Ariti, A. M.; Geleto, S. A.; Gutema, B. T.; Mekonnen, E. G.; Workie, Y. A.; Abda, E. M.; Mekonnen, M. L. Magnetite chitosan hydrogel nanozyme with intrinsic peroxidase activity for smartphone-assisted colorimetric sensing of thiabendazole. *Sensing and Bio-Sensing Research* **2023**, *42*, No. 100595.
(3) Gao, L.; Zhuang, J.; Nie, L.; Zhang, J.; Zhang, Y.; Gu, N.; Wang, T.; Feng, J.; Yang, D.; Perrett, S.; Yan, X. Intrinsic peroxidase-like activity of ferromagnetic nanoparticles. *Nat. Nanotechnol* **2007**, *2* (9), 577−83.
(4) Mekonnen, E. G.; Shitaw, K. N.; Hwang, B.-J.; Workie, Y. A.; Abda, E. M.; Mekonnen, M. L. Copper nanoparticles embedded fungal chitosan as a rational and sustainable bionanozyme with robust laccase activity for catalytic oxidation of phenolic pollutants. *RSC Adv.* **2023**, *13* (46), 32126−32136.
(5) Kim, M. Y.; Kim, J. Chitosan Microgels Embedded with Catalase Nanozyme-Loaded Mesocellular Silica Foam for Glucose-Responsive Drug Delivery. *ACS Biomater Sci. Eng.* **2017**, *3* (4), 572−578.
(6) Nagvenkar, A. P.; Gedanken, A. Cu0.89Zn0.11O, A New Peroxidase-Mimicking Nanozyme with High Sensitivity for Glucose and Antioxidant Detection. *ACS Appl. Mater. Interfaces* **2016**, *8* (34), 22301−8.
(7) Shen, X.; Liu, W.; Gao, X.; Lu, Z.; Wu, X.; Gao, X. Mechanisms of Oxidase and Superoxide Dismutation-like Activities of Gold, Silver, Platinum, and Palladium, and Their Alloys: A General Way to the Activation of Molecular Oxygen. *J. Am. Chem. Soc.* **2015**, *137* (50), 15882−91.
(8) Liang, M.; Yan, X. Nanozymes: From New Concepts, Mechanisms, and Standards to Applications. *Acc. Chem. Res.* **2019**, *52* (8), 2190−2200.
(9) Wang, P.; Wang, T.; Hong, J.; Yan, X.; Liang, M. Nanozymes: A New Disease Imaging Strategy. *Front. Bioeng. Biotechnol.* **2020**, *8*, 15.
(10) Chow, A.Y. Cell cycle control by oncogenes and tumor suppressors: driving the transformation of normal cells into cancerous cells. *Nat. Educ.* **2010**, *3* (9), 7.
(11) Alula, M. T.; Feke, K. Peroxidase-Like Activity of Silver Nanoparticles Loaded Filter Paper and its Potential Application for Sensing. *Journal of Cluster Science* **2023**, *34* (1), 613−621.
(12) Ankala, B. A.; Achamyeleh, A. A.; Abda, E. M.; Workie, Y. A.; Su, W.-N.; Wotango, A. S.; Mekonnen, M. L. MoS2/Cu as a peptide/nucleotide-matrix-free laccase memetic nanozyme for robust catalytic oxidation of phenolic pollutants. *New J. Chem.* **2023**, *47*, 19880.
(13) Mehrabani, M. G.; Karimian, R.; Rakhshaei, R.; Pakdel, F.; Eslami, H.; Fakhrzadeh, V.; Rahimi, M.; Salehi, R.; Kafil, H. S. Chitin/silk fibroin/TiO(2) bio-nanocomposite as a biocompatible wound dressing bandage with strong antimicrobial activity. *Int. J. Biol. Macromol.* **2018**, *116*, 966−976.
(14) Levy, S. B.; Marshall, B. Antibacterial resistance worldwide: causes, challenges and responses. *Nature Medicine* **2004**, *10* (12), S122−S129.
(15) Akram, F.; Imtiaz, M.; Haq, I. U. Emergent crisis of antibiotic resistance: A silent pandemic threat to 21st century. *Microbial Pathogenesis* **2023**, *174*, No. 105923.
(16) Fang, G.; Kang, R.; Cai, S.; Ge, C. Insight into nanozymes for their environmental applications as antimicrobial and antifouling agents: Progress, challenges and prospects. *Nano Today* **2023**, *48*, No. 101755.
(17) Lulseged, K.; Akele, M. Z.; Abiye, A. A.; Abebe, B.; Assefa Huluka, S. Wound Healing and Antioxidant Properties of 80% Methanol Leaf Extract of Verbascum sinaiticum (Scrophulariaceae): An Ethiopian Medicinal Plant. *Evid. Based Complement. Alternat. Med.* **2022**, *2022*, No. 9836773.
(18) Cao, F.; Zhang, L.; You, Y.; Zheng, L.; Ren, J.; Qu, X. An Enzyme-Mimicking Single-Atom Catalyst as an Efficient Multiple Reactive Oxygen and Nitrogen Species Scavenger for Sepsis Management. *Angew. Chem., Int. Ed.* **2020**, *59* (13), 5108−5115.
(19) Li, G.; Liu, H.; Hu, T.; Pu, F.; Ren, J.; Qu, X. Dimensionality Engineering of Single-Atom Nanozyme for Efficient Peroxidase-Mimicking. *J. Am. Chem. Soc.* **2023**, *145* (30), 16835−16842.
(20) Bilalis, P.; Karagouni, E.; Toubanaki, D. K. Peroxidase-like activity of Fe3O4 nanoparticles and Fe3O4-graphene oxide nanohybrids: Effect of the amino- and carboxyl-surface modifications on H2O2 sensing. *Appl. Organomet. Chem.* **2022**, *36* (9), No. e6803.
(21) Li, Z.; Yang, X.; Yang, Y.; Tan, Y.; He, Y.; Liu, M.; Liu, X.; Yuan, Q. Peroxidase-Mimicking Nanozyme with Enhanced Activity and High Stability Based on Metal-Support Interactions. *Chemistry* **2018**, *24* (2), 409−415.
(22) Williams, S.; Okolie, C. L.; Deshmukh, J.; Hawco, L.; McNeil, J.; Nganou Assonkeng, A. C.; Bennett, C.; Mkandawire, M. Magnetizing Cellulose Fibers with CoFe(2)O(4) Nanoparticles for Smart Wound Dressing for Healing Monitoring Capability. *ACS Appl. Bio Mater.* **2019**, *2* (12), 5653−5662.
(23) Siemianowicz, K.; Bajor, G.; Likus, W. Nanosilver - does it have only one face? *Acta Biochim. Pol.* **2013**, *60*(4), DOI: 10.18388/abp.2013_2013.
(24) Mekonnen, M. L.; Mola, A. M.; Abda, E. M. Rapid Colorimetric Detection of Thiabendazole Based on Its Inhibition Effect on the Peroxidase Mimetic Activity of Ag-MoS2 Nanozyme. *ACS Agric Sci. Technol.* **2023**, *3* (1), 82−89.
(25) Zhang, L.; Wang, H.; Qu, X. Biosystem-Inspired Engineering of Nanozymes for Biomedical Applications. *Adv. Mater.* **2023**, No. 2211147.
(26) Zhang, R.; Yan, X.; Fan, K. Nanozymes Inspired by Natural Enzymes. *Acc. Mater. Res.* **2021**, *2* (7), 534−547.
(27) Trache, D.; Tarchoun, A. F.; Derradji, M.; Hamidon, T. S.; Masruchin, N.; Brosse, N.; Hussin, M. H. Nanocellulose: From Fundamentals to Advanced Applications. *Front. Chem.* **2020**, *8*, 392 DOI: 10.3389/fchem.2020.00392.
(28) Yu, N.; Cai, T.; Sun, Y.; Jiang, C.; Xiong, H.; Li, Y.; Peng, H. A novel antibacterial agent based on AgNPs and Fe(3)O(4) loaded chitin microspheres with peroxidase-like activity for synergistic antibacterial activity and wound-healing. *Int. J. Pharm.* **2018**, *552* (1−2), 277−287.
(29) Sannino, A.; Demitri, C.; Madaghiele, M. Biodegradable Cellulose-based Hydrogels: Design and Applications. *Materials* **2009**, *2* (2), 353−373.
(30) Krainer, F. W.; Glieder, A. An updated view on horseradish peroxidases: recombinant production and biotechnological applications. *Appl. Microbiol. Biotechnol.* **2015**, *99* (4), 1611−1625.
(31) Worku, L. A.; Bachheti, R. K.; Tadesse, M. G.; Perez, V. H. Isolation and Characterization of Natural Cellulose from Oxytenanthera abyssinica (Lowland Ethiopian Bamboo) Using Alkali Peroxide Bleaching Stages Followed by Aqueous Chlorite in Buffer Solution. *Int. J. Poly Sci.* **2022**, *2022*, No. 5155552.
(32) Abdul Rahman, N. H.; Chieng, B. W.; Ibrahim, N. A.; Abdul Rahman, N., Extraction and Characterization of Cellulose Nanocrystals from Tea Leaf Waste Fibers. *Polymers (Basel)* **2017**, *9* (11), 588, DOI: .

(33) Bacha, E. G.; Demsash, H. D. Extraction and Characterization of Nanocellulose from Eragrostis Teff Straw. *Research Square*: **2021**; Vol. Version 1.

(34) Wang, G.; Li, F.; Li, L.; Zhao, J.; Ruan, X.; Ding, W.; Cai, J.; Lu, A.; Pei, Y. In Situ Synthesis of Ag-Fe(3)O(4) Nanoparticles Immobilized on Pure Cellulose Microspheres as Recyclable and Biodegradable Catalysts. *ACS Omega* **2020**, *5* (15), 8839−8846.

(35) Taheri, S.; Heravi, M. M.; Saljooqi, A. Ionothermal synthesis of magnetic N-doped porous carbon to immobilize Pd nanoparticles: An efficient heterogeneous catalyst for reduction of nitroaromatic compounds. *Sci. Rep.* **2022**, *13*, No. 17566, DOI: 10.1038/s41598-023-35998-5.

(36) Workie, Y. A.; Sabrina; Imae, T.; Krafft, M. P. Nitric oxide gas delivery by fluorinated poly (Ethylene Glycol)@ graphene oxide carrier toward pharmacotherapeutics. *ACS Biomaterials Science & Engineering* **2019**, *5* (6), 2926−2934.

(37) Sauer, U. G.; Hill, E. H.; Curren, R. D.; Raabe, H. A.; Kolle, S. N.; Teubner, W.; Mehling, A.; Landsiedel, R. Local tolerance testing under REACH: Accepted non-animal methods are not on equal footing with animal tests. *Altern. Lab. Anim.* **2016**, *44* (3), 281−299.

(38) Gond, R. K.; Gupta, M. K.; Jawaid, M. Extraction of nanocellulose from sugarcane bagasse and its characterization for potential applications. *Polym. Compos* **2021**, *42* (10), 5400−5412.

(39) Pant, B.; Park, M.; Lee, J. H.; Kim, H. Y.; Park, S. J. Novel magnetically separable silver-iron oxide nanoparticles decorated graphitic carbon nitride nano-sheets: A multifunctional photocatalyst via one-step hydrothermal process. *J. Colloid Interface Sci.* **2017**, *496*, 343−352.

https://doi.org/10.1021/acsomega.3c05748
ACS Omega 2023, 8, 48764−48774